Materials Today Bio 33 (2025) 101962

Contents lists available at ScienceDirect

Materials Today Bio

journal homepage: www.journals.elsevier.com/materials-today-bio

Virtual testing methodology to predict the mechanical behavior of collagen hydrogels from nanoarchitecture

Elías Núñez-Ortega [a,b], Pablo Blázquez-Carmona [c], Raquel Ruiz-Mateos [a,b], José E. Martín-Alfonso [d], José A. Sanz-Herrera [a,b,1], Esther Reina-Romo [a,b,*,1]

[a] Escuela Técnica Superior de Ingeniería, Universidad de Sevilla, Avenida Camino de los Descubrimientos s/n, 41092, Sevilla, Spain
[b] Instituto de Biomedicina de Sevilla (IBIS), C. Antonio Maura Montaner, 41013, Sevilla, Spain
[c] Departamento de Ingeniería Mecánica y Diseño Industrial, Escuela Superior de Ingeniería, Universidad de Cádiz, Avenida Universidad de Cádiz 10, 11519, Puerto Real, Cádiz, Spain
[d] Centro de Investigación en Tecnología de Productos y Procesos Químicos (Pro^{2}TecS), Departamento de Ingeniería Química y Ciencia de los Materiales, Escuela Técnica Superior de Ingeniería, Universidad de Huelva, Avenida de las Fuerzas Armadas s/n, 21007, Huelva, Spain

ARTICLE INFO

Keywords:
Collagen-based hydrogels
FIB-SEM
Fiber structures
Homogenization
In silico model
Mechanobiology
Rheology

ABSTRACT

Collagen-based hydrogels are three-dimensional, cross-linked structures capable of mimicking the extracellular fibered matrix of biological tissues, making them particularly well-suited for biomedical applications. These hydrogels typically exhibit highly non-linear mechanical behavior, which strongly depends on their internal nanostructural characteristics - an interconnection that remains poorly understood. The aim of this work is to combine high resolution imaging with a multiscale *in silico* structural model to virtually reproduce the mechanical behavior of a widely used collagen-based hydrogel, using solely its nanoarchitecture as input. The real fiber structure of the hydrogel was originally quantified at the nanometer scale using state-of-the-art microscopy, specifically, focused ion beam-scanning electron microscopy (FIB-SEM). *In silico* shear tests were then performed on the reconstructed collagen matrix to compute, through a multiscale approach, its homogenized mechanical response, including the energies and stresses developed by the fibers during the tests. Different samples of the hydrogel were also mechanically characterized by means of rheological tests to fit the model and show the feasibility of the methodology. The *in silico* simulations successfully captured the detailed mechanical interactions between fibers as well as the experimental non-linear mechanical behavior of the hydrogels. Results also highlight the relevant role of the bending energy throughout the entire range of deformation analyzed. This methodology provides a framework to elucidate the structure-mechanical behavior relationship of fiber network topologies, and can be applied to predict mechanical response of both native tissues and biomaterials based exclusively on their fibered nanostructures.

1. Introduction

Biological tissues of the human body perform crucial physiological functions. Their cellular and mechanical behavior is strongly influenced by their fibrous composition, especially by the 3D structural arrangement and the concentration of the fibers [1]. Collagen is among the most abundant fibrous proteins in mammals and provides an essential support for the extracellular matrix (ECM) [2–5]. According to its nanostructural organization, collagen fibers can provide significant tensile strength, enabling tissues to resist stretching, along with a certain degree of flexibility. In addition to providing mechanical support, collagen is involved in various cellular processes such as cell attachment, cell migration or tissue development and repair. Moreover, this fiber network might change its geometry and its mechanical response due to drugs, ageing and disease. For example, in cardiovascular diseases like aortic dissection, evidence suggests that medial weakness caused by a significant reduction in interlaminar elastic fibers contributes to the development of the dissection [6]. In aortic aneurysms, fiber degradation and fragmentation are also observed [7], and the elastin content significantly decreases as the aneurysm diameter increases [8]. In

* Corresponding author. Avenida Camino de los Descubrimientos s/n, 41092-Sevilla, Spain.
E-mail addresses: enunez3@us.es (E. Núñez-Ortega), pablo.blazquez@uca.es (P. Blázquez-Carmona), rruiz-mateos@us.es (R. Ruiz-Mateos), jose.martin@diq.uhu.es (J.E. Martín-Alfonso), jsanz@us.es (J.A. Sanz-Herrera), erreina@us.es (E. Reina-Romo).
[1] Joint senior authorship.

https://doi.org/10.1016/j.mtbio.2025.101962
Received 18 March 2025; Received in revised form 20 May 2025; Accepted 6 June 2025
Available online 9 June 2025

osteoarthritis, a degenerative joint disease, cartilage undergoes structural changes in the collagen network [9–11], including collagen reorientation [9,12], collagen degradation, changes in interconnectivity [13] and a reduction in the collagen content [14]. During cancer, the extracellular matrix undergoes a dysregulated remodeling, including both fiber deposition and degradation [15]. Normally, aligned and often thickened fibers are associated with tissue fibrosis and tumor progression [16]. Therefore, to advance in the development of predictive models with enhanced physiological relevance, *in vitro* and *in silico* models need to capture and replicate these nanoscale interactions in the fibered structure of biological tissues.

A significant amount of *in vitro* research is now focused on designing biomaterials that replicate key characteristics of the tissue microenvironment [17–20]. In this context, the use of collagen-based hydrogels for 3D healthy and disease tissue modeling is a popular approach due to their ability to mimic realistic tissue stiffness and composition [21–23]. Collagen-based hydrogels are non-linear viscoelastic materials, whose mechanical behavior is strongly influenced by their nanostructure. Their mechanical properties depend on factors such as collagen type, the concentration, which affects hydrogel's density and stability, and the crosslinking method, that varies its strength [24]. The manufacturing conditions, including the polymerization temperature, pH and ionic strength, also affect their structural and mechanical properties [25]. Since mechanical properties regulate cell behavior and are essential for biomedical applications, studying and optimizing them according to the specific requirements of each application is crucial [24–26]. In this context, rheology is a suitable tool for monitoring the evolution of hydrogels during polymerization or under physiological conditions, as well as for understanding how they respond to macroscopic shear stresses and strains, providing information about their mechanical performance [27,28].

In addition to experimental testing, computational models provide valuable tools for simulating and predicting the mechanical behavior of fibered matrices. These models are mainly classified as continuum or discrete (see Ref. [29] for a review). Continuum models study the overall network behavior from a phenomenological perspective by homogenizing fiber properties without explicitly incorporating their individual geometries or interactions [29,30]. They employ polynomial [31], exponential [32] or logarithmic [33] functions, among others, to express the strain energy density and simulate the apparent network's mechanical behavior, requiring experimental data to fit model variables. In the context of collagen hydrogels, Lane et al. [34] conducted unconfined compression tests using continuum models with four different strain energy functions. Castro et al. [35] employed a poroelastic continuum finite element (FE) model, describing the hydrogel's isotropic hyperelasticity in terms of shear and bulk moduli. In a further study, Castro et al. [36] simulated the non-linear mechanical behavior of hydrogels under confined compression, varying the hyperelastic model formulation and using two distinct FE solvers. In summary, continuum models present the advantage of being a useful approximation for reproducing the mechanical response of fibrous networks, avoiding the complexity of considering each fiber individually. However, they have limitations in modeling complex deformations and do not provide detailed information about the network's micro- or nanostructure.

On the other hand, discrete models are able to represent the micro- or nanostructure of fiber networks by modeling individual fiber components. A common approach is simulating random 2D or 3D fiber networks [29], where fiber interactions may be omitted [37,38] or modeled using different methods, including beam [39], welded [40] crosslinks, or springs [41,42]. These models simulate networks with fibers represented as straight or wavy segments. However, since these networks are randomly generated, they do not replicate real geometries. For example, Sanz-Herrera et al. [43] developed a multiscale formulation to study the mechanical behavior of curved fibrous networks. After evaluating the mechanics of a single fiber, the authors proposed a model to generate fibered matrices based on desired fiber density and geometry, which were then subjected to tensile, compression and shear tests. Another approach involves generating models from images obtained by computed tomography (CT) [44,45], confocal microscopy [46,47] or scanning electron microscopy (SEM) [48]. These techniques produce networks that replicate fibrous structures with varying levels of detail or enable the creation of artificial networks based on real network data. For instance, Lindström et al. [46] used confocal microscopy on type-I collagen to develop a fibrous network representation through skeletonization, which was subsequently transformed into random artificial networks using a Euclidean graph generation algorithm. These two types of networks did not account for some structural effects, such as tortuosity of fibers or fiber interactions, among others, and were analyzed in shear tests exhibiting similar behavior only in the elastic regime. While some authors found that network strength does not depend on fiber tortuosity [49], these features do influence the transition from linear to non-linear behavior, thus modulating the strain stiffening of the system, although the effect becomes negligible when the network is embedded in an elastic matrix [50]. Regarding collagen hydrogels, Olivares et al. [47] reconstructed 3D collagen networks from confocal images, obtaining parameters such as fiber orientation, fiber length and pore size, although mechanical tests were not performed.

In the present work, a novel methodology is proposed with the aim of virtually reproducing the mechanical behavior of collagen structures using their nanostructures as input of the computer algorithm. This approach incorporates the real structure of a collagen-based hydrogel, considering the different lengths, tortuosities and interconnections of its fibers. For this purpose, focused ion beam-scanning electron microscopy (FIB-SEM) was employed to precisely reconstruct the intricate fibrous microstructure at the nanometer scale. From the FIB-SEM images, the hydrogel's nanoarchitecture was characterized, enabling the reconstruction of its real fibered matrix. A multiscale *in silico* model was then applied to reproduce the experimental mechanical response obtained in rheological tests performed on collagen-based hydrogels. The *in silico* simple shear tests were conducted on the reconstructed fibered matrix, calculating mechanical responses, fiber stresses and strain energy densities, providing a comprehensive understanding of the fibrous networks' behavior.

2. Materials and methods

2.1. Preparation of collagen-based hydrogels

Hydrogels were prepared using type-I collagen fibrils as the primary structural component, at a final concentration (C) of 0.8 mg/mL. The commercial collagen was extracted from bovine dermis through an acidification process and supplied at a stock concentration of 4.0 mg/mL (Collagen-G; Matrix Bioscience, Deutschland, Germany). Collagen mixtures were prepared in 1 mL volumes inside 50 mL conical tubes, with all reagents and pipette tips kept on ice to prevent an early hydrogel polymerization. Polymerization was initiated *in vitro* by adjusting the pH to 7.4 using 1 M NaOH (Sigma-Aldrich, Missouri, USA), which triggered the self-assembling of collagen fibrils into bundled fibers, forming a matrix structure. The solution was also buffered with 0.36 M $NaHCO_3$ (Merck KGaA, Darmstadt, Germany), and mixed with Dulbecco's modified Eagle's medium (Gibco, Thermo Fisher Scientific, Waltham, Massachusetts, USA), as shown in Fig. 1A. These components also served as aqueous solvents, providing the hydrated environment essential for hydrogel formation. The hydrogels were then allowed to polymerize at 37 °C, pre-mounted in a 35 mm petri dish, for 1 hr in an incubator. A schematic of the collagen hydrogel polymerization is also presented in Fig. 1A, along with a SEM image of the resulting bovine collagen-based hydrogel, highlighting its fibrous network structure.

2.2. Rheological tests

The shear strain-stress relationship of collagen hydrogels was

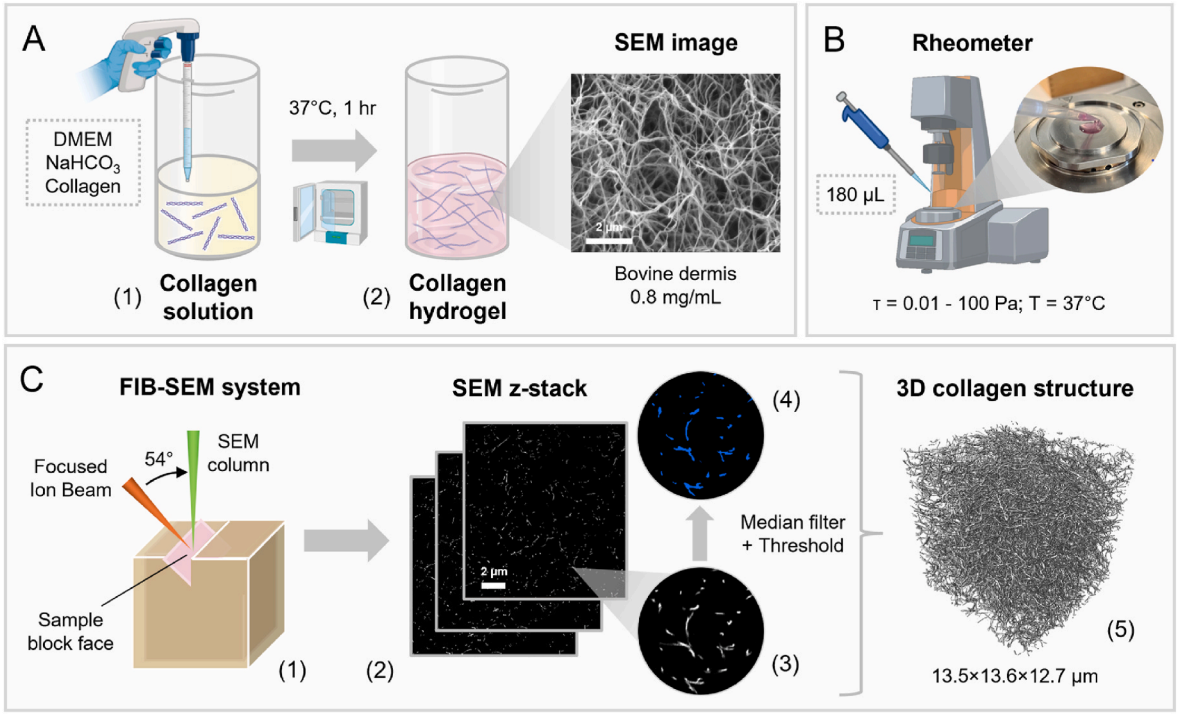

Fig. 1. Summary of the experimental procedure and FIB-SEM image processing results. A) Schematic representation of the bovine collagen-based hydrogel preparation, showing the initial collagen solution (1) and the polymerized collagen hydrogel (2), along with a SEM image of the fibrous architecture. Scale bar is 2 µm. B) Schematic representation of the rheometer setup, including a detailed view of the sample deposition. C) Schematic of the FIB-SEM system (1), examples of acquired FIB-SEM images (2), an image after applying median filtering (3) and interactive thresholding (4), and 3D collagen structure generated after thresholding the complete set of FIB-SEM images (5).

measured using small-amplitude oscillatory shear (SAOS) tests. Collagen hydrogels inherently exhibit viscoelastic behavior governed by the collagen fibers [28,51–53], combining both elastic and viscous responses. This makes SAOS testing particularly well-suited for characterizing their mechanical properties. These experiments were conducted using a stress-controlled rotational rheometer (MCR 301; Anton Paar, Graz, Austria) at 37 °C, employing a standard steel cone geometry (CP25-1) with a diameter of 25 mm and an angle of 1°, and a standard Peltier plate. Hydrogels were prepared as described in Section 2.1 (maintaining the same collagen concentration of 0.8 mg/mL in all of them) and, immediately after mixing, 180 µL were loaded at the center of the rheometer's Peltier plate. The cone plate was then positioned at a gap height of 48 µm. Excess hydrogel that overflowed from the device was removed using a flat-ended micro spatula. Silicone oil was subsequently applied around the cone perimeter to minimize sample drying during the test. The polymerization of the hydrogels was assessed *in situ* by monitoring the evolution of the storage modulus (G') and the loss modulus (G'') over time under constant stress amplitude and frequency. The strain (1 %) and frequency (1 Hz) values were determined from preliminary strain and frequency sweeps to ensure they remained well below the yield strain and exceeded the crossover frequency, respectively.

Once the viscoelastic properties stabilized after 1 hr of polymerization, a stress-strain test was performed. Thus, stress-controlled rotation was conducted using a logarithmic ramp profile, a standard approach in rheological analysis when broad stress intervals are involved. Shear stress was varied from 0.01 to 100 Pa, evaluating the strain at 20 points per decade. Data acquisition and analysis were performed using RHEOPLUS/32 software (Anton Paar, Graz, Austria). The test was repeated two times for different samples ($n = 2$). A schematic of the rheometer setup and a detailed view of the hydrogel deposition are shown in Fig. 1B.

2.3. FIB-SEM image acquisition

The nanoscale structure of the collagen hydrogels (0.8 mg/mL concentration) was analyzed using focused ion beam milling and scanning electron microscopy (FIB-SEM) [54,55], a technique that allows for the segmentation of a 3D fibrous network and precise measurement of structural parameters [56].

First, 100 µL of the hydrogel was prepared following the protocol outlined in Section 2.1. The sample preparation procedure for FIB-SEM was based on the method developed by Serra Lleti [57], with slight modifications introduced to improve contrast and reduce sample charging and imaging artifacts, as detailed below. After polymerization, it was fixed in 2.5 % glutaraldehyde with 0.1 M cacodylate-HCl buffer (pH 7.4) at 4 °C for 2 hr. Following fixation, samples were rinsed three times with 0.1 M cacodylate-HCl buffer. To enhance the contrast of the collagen fibers, a post-fixation treatment was applied, involving several incubation steps in the following solutions: 2 % osmium tetroxide and 1.5 % potassium ferrocyanide (1.5 hr), 1 % thiocarbohydrazide (30 min), 2 % osmium tetroxide (1 hr), 4 % uranyl acetate (10 hr), and 1 % lead aspartate (1 hr). This treatment was carried out at room temperature, with washes in distilled water between every step. Dehydration was subsequently performed using a graded acetone series (50 %–100 %). The sample was finally embedded in hydrophobic Durcupan ACMTH resin (Sigma-Aldrich, Missouri, USA).

Later, samples were mounted onto standard SEM pin stubs. A conductive surface was achieved by coating the samples with a 30 nm layer of gold/palladium alloy (80/20). Images were acquired using a Zeiss Crossbeam 550 microscope (ZEISS, Oberkochen, Germany) equipped with a Xe/Ga ion source. The FIB-SEM system was configured at a 54° tilt to align the SEM and FIB columns (Fig. 1C; detail 1). Therefore, the coincidence point was located at a working distance of 5.2 mm. A 15 × 15 µm area on the resin block surface was selected, and a 1-µm-thick platinum protective layer was deposited using the electron

beam for 5 min to safeguard the sample. Autotuning and tracking marks were etched into this layer to minimize curtaining artifacts during FIB milling and to correct alignment errors during post-processing. The FIB-SEM process involved iterative slicing and polishing of the embedded hydrogel, with high-resolution images captured for each layer (pixel size: 9.37 × 9.37 nm in x- and y-axis, and 20.21 nm in z-axis; see detail 2 in Fig. 1C). The complete set of FIB-SEM images of the hydrogel can be seen in Video SM1 in the supplementary material.

2.4. Hydrogel nanostructure generation

To reconstruct the nanostructure of the collagen-based hydrogels, the FIB-SEM images described in Section 2.3 (Fig. 1C; detail 2) were used. The FIB-SEM images were analyzed using Avizo software (Thermo Fisher Scientific, Waltham, Massachusetts, USA). First, a median filtering was applied to diminish the noise while retaining the integrity of the fiber edges, considering a 3D interpretation with 18 neighboring pixels (Fig. 1C; detail 3). Then, an interactive thresholding was set for the fibers, with an intensity range between 40 and 255 (Fig. 1C; detail 4). The resulting 3D collagen structure is shown in Fig. 1C (detail 5).

Three inner volumes of interest (VOIs), each approximately 4.7 × 4.7 × 5.1 μm, were defined to encompass different parts of the collagen structure, while minimizing the boundary edge effects. The selected VOIs and their corresponding 3D structures are shown in Fig. 2A and B, respectively. Moreover, small spots of residual noise, each less than 1000 pixels in size, were removed from each VOI using the plugin *Remove Small Spots*.

The 3D fibered structure of each VOI was skeletonized using the plugin *Filament Editor*, which enables the modeling of fibered structures as lines with a certain thickness. In this way, the fibers were divided into segments of variable lengths, each discretized into multiple points. Fig. 2C displays the skeletonized fibered structure (spatial network)

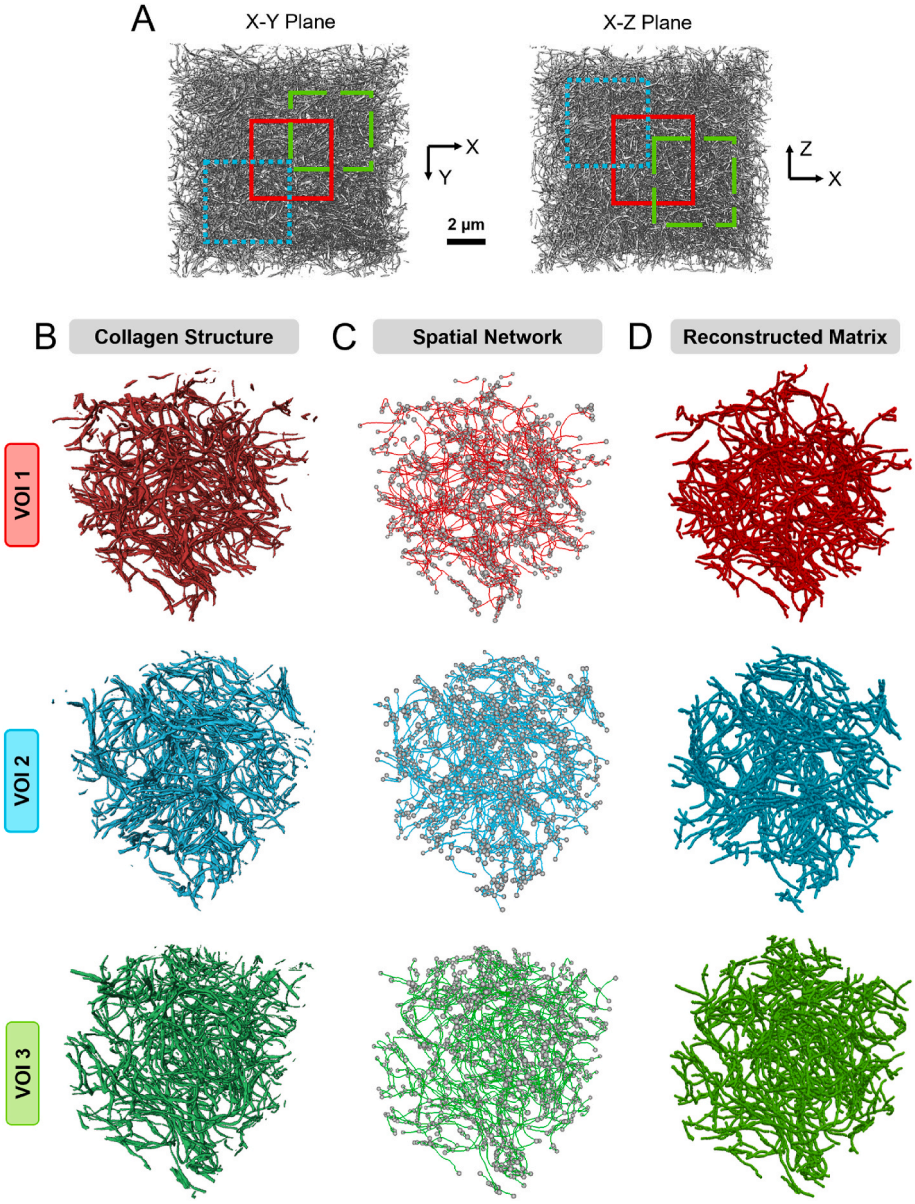

Fig. 2. Summary of the methodology followed to reconstruct the nanostructure of collagen-based hydrogels. A) Selection of three different volumes of interest (approximately 4.7 × 4.7 × 5.1 μm) within the complete collagen structure in the X-Y and X-Z planes (scale bar is 2 μm in both views). For each selected volume of interest: B) 3D collagen structure; C) spatial network after skeletonizing the 3D collagen structure (nodes in gray and segments in red, blue and green for VOI 1, 2 and 3, respectively); and D) visualization of the reconstructed fibered matrix (it can be observed that the fibered matrix coincides, without including isolated segments, with the collagen structure).

obtained from each VOI. These spatial networks were subsequently extracted, including the coordinates of all points, the points composing the segments, and the initial and final nodes of each segment. Finally, using the *Spatial Graph Statistics* module, geometrical parameters such as total segment length (L_s), length between endpoints (L), tortuosity (T) and orientation were obtained for each segment of the spatial networks. In this context, tortuosity is defined as the ratio between the total length and the endpoint length of a segment:

$$T = L_s / L \tag{1}$$

Segment orientations were characterized by means of two angular components: φ and θ. Orientation φ represents the azimuthal angle in the X-Y plane (calculated from the X-axis to the Y-axis), ranging from 0° to 360°. In contrast, orientation θ describes the elevation angle between the segment and the Z-axis. This angle varies from 0°, indicating a segment perpendicular to the X-Y plane, to 90°, when the segment is parallel to it. Other alternative methods, such as Fourier transform-based indicators to characterize fiber orientation distribution and anisotropy [58], could be employed.

Regarding fiber thickness, this parameter can be computed as an output of the FIB-SEM analysis by extracting the mean radius of the segments. However, some studies suggest that these values may not reflect the true fiber thickness, as they are obtained from dehydrated samples [59,60]. Consequently, this parameter has been omitted in this work.

A comparison of the extracted data from the three VOIs is provided in Table 1 and Figs. SM1 and SM2 in the supplementary material. Table 1 shows that the skeletonization of different volumes resulted in a comparable number of segments, points and nodes. It also indicates that the geometrical metrics of the VOIs had similar mean and standard deviation values. Furthermore, the overall standard deviations of the connectivity metrics are negligible. Figs. SM1 and SM2 highlight a general similarity in the histograms of the geometrical parameters across the VOIs. Together, these results demonstrate that the three selected VOIs exhibit similar characteristics, suggesting that they are representative spatial networks of the hydrogels' nanoarchitecture.

Considering the number of segments in each VOI, the segment density (an indirect representation of fiber density) was obtained by taking into account their total volumes (111.8 μm^3). Based on this ratio, the collagen concentration-segment density relationship was determined. The resulting values were $4.24 \cdot 10^{-14}$ mg/segment, $4.32 \cdot 10^{-14}$ mg/segment and $4.20 \cdot 10^{-14}$ mg/segment for VOIs 1, 2 and 3, respectively, showing very small variation among them.

Finally, the spatial network data extracted from Avizo (point coordinates, segment points and initial and final nodes) were processed in Matlab (MathWorks, Natick, Massachusetts, USA) to generate the fibered matrices of the three VOIs. This processing removed the isolated segments from the networks, as these would have negligible influence on the shear test results, and generated files containing the final coordinates, elements (connections between points) and nodes. Using these coordinates and elements, the reconstructed fibered matrices of the considered VOIs were visualized in ParaView (Kitware, Clifton Park, New York, USA), as shown in Fig. 2D. Upon examining the visualizations, it was confirmed that the resulting fibered matrices coincided (excluding the isolated segments) with the collagen structures obtained from Avizo (see Fig. 2B and D).

2.5. *In silico simple shear tests*

The methodology proposed by Sanz-Herrera et al. [43] was used to simulate the experimental results of the rheological tests on the bovine collagen-based hydrogels prepared in Section 2.1. In their work, fibered structures were modeled using 3D Euler-Bernoulli beam elements (3 translations + 3 rotations) in an updated Lagrangian scheme [43]. The resulting multiscale model enables the analysis of the micromechanical interactions between fibers to determine the macroscopic mechanical behavior of fibered matrices. Thus, a set of different matrices was generated and subsequently subjected to *in silico* tensile/compression and simple shear tests [43]. In the present study, the same methodology was employed to perform virtual simple shear tests on the reconstructed fibered matrices of the considered VOIs.

The input data required for the model (see Ref. [43] for a complete description) include the coordinates, elements and nodes of each VOI, obtained after processing the data extracted from Avizo. Moreover, to perform the simple shear test on each reconstructed fibered matrix, the axial and bending stiffnesses of the fibers were adjusted to ensure that the resulting mean curve closely matched the experimental curves.

The bending and axial stiffnesses, k_b and k_a, respectively, can be defined by the following equations:

$$k_b = E_f \cdot I_f \tag{2}$$

$$k_a = E_f \cdot A_f \tag{3}$$

where E_f is the Young's modulus of the collagen fibers, I_f is the second moment of inertia of the cross-section and A_f is the cross-sectional area of the fibers. I_f and A_f are interpreted in the present study as apparent or effective properties, given the hierarchical and multiscale nature of collagen fibers [61]. Therefore, instead of using fiber diameter to obtain these quantities, they should be computed through the interaction of fibrils and crosslinks at different spatial scales.

In addition to obtaining the shear stress-strain curves of the selected VOIs, the total, axial, bending and torsional accumulated strain energy densities were calculated for each case analyzed, as well as the total, axial and bending stresses developed for the elements of the segments that composed the fibers.

3. Results and discussion

3.1. *Rheological tests reveal the highly non-linear mechanical behavior of the collagen hydrogels*

The bovine collagen-based hydrogels with a concentration of 0.8 mg/mL were subjected to rheological tests following the procedure described in Section 2.2. Fig. 3B plots the experimental results obtained

Table 1
Comparison of the selected volumes of interest in terms of connectivity (number of segments, points and nodes) and geometrical metrics (mean (standard deviation) of total segment length, endpoint length, tortuosity, azimuthal angle and elevation angle of the segments). Overall mean (standard deviation) is also provided for both connectivity and geometrical metrics.

	Metric	VOI 1	VOI 2	VOI 3	Mean (SD)
Connectivity Metrics	Number of Segments	2108	2070	2128	2102 (29)
	Number of Points	54467	53117	56438	54674 (1670)
	Number of Nodes	1710	1751	1766	1742 (29)
Geometrical Metrics	Total Segment Length, L_s [nm]	341.30 (339.37)	348.16 (329.69)	350.18 (346.83)	346.55 (338.75)
	Endpoint Length, L [nm]	298.86 (284.27)	304.78 (276.37)	304.47 (289.25)	302.70 (283.37)
	Tortuosity, T [−]	1.13 (0.31)	1.14 (0.32)	1.14 (0.31)	1.13 (0.31)
	Azimuthal Angle, φ [°]	164.33 (106.00)	170.67 (98.13)	174.13 (101.11)	169.72 (101.88)
	Elevation Angle, θ [°]	56.23 (22.42)	53.43 (22.67)	55.17 (22.69)	54.95 (22.62)

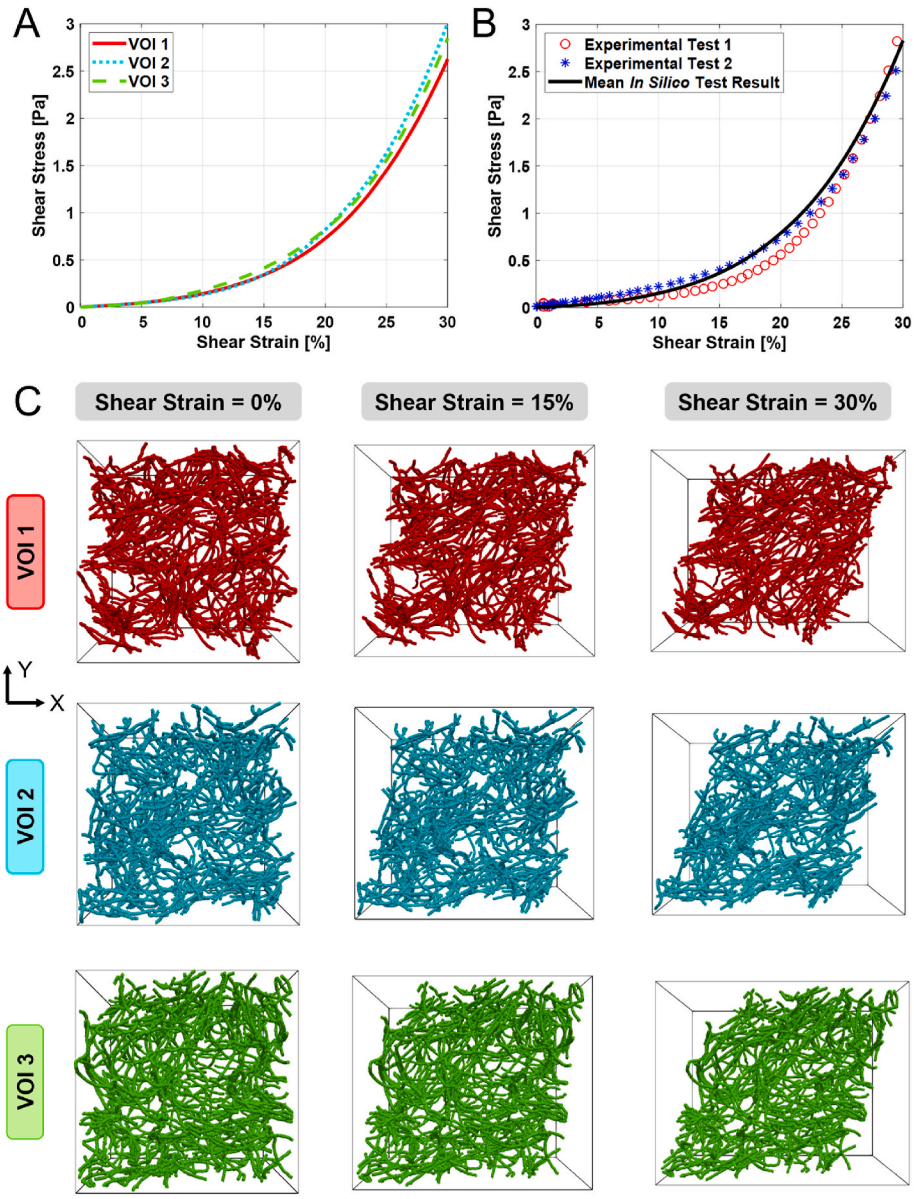

Fig. 3. Results of the rheological tests performed. A) Result of the *in silico* simple shear test for each volume of interest. B) Comparison of experimental results (represented by markers) and *in silico* results (represented by the mean curve). C) State of the fibered matrix of the volumes of interest before (shear strain = 0 %), during (shear strain = 15 %) and after (shear strain = 30 %) applying the *in silico* simple shear test.

for each test, up to a maximum shear strain of 30 %. The results show consistent trends across the different tests, with shear stress values ranging between 0 and 3 Pa. Moreover, the tests capture the non-linear mechanical behavior characteristic of this type of collagen tissues. Initially, a region with approximately linear behavior is observed up to 10–15 % shear strain. This linearity shifts to non-linear behavior, likely due to the progressive alignment and stretching of collagen fibers in the direction of the applied load.

These experimental results are consistent with other findings reported in the literature [62,63]. For instance, the results (Fig. 3B) are in line with those obtained by Arevalo et al. [62], who performed rheological tests on a two-layer system consisting of polyacrylamide and rat tail type-I collagen gels, with varying collagen concentrations in the range of 0.25–1.5 mg/mL. In their study, an approximately linear response could be observed at the beginning of the tests, followed by a non-linear increase in shear stress as the tests progressed, which was attributed to the network's realignment in the shear direction. This behavior is in agreement with the present observations, with differences in the shear stress-strain curves probably due to factors such as collagen source, collagen concentration or polymerization temperature, among others.

3.2. *In silico shear stress-strain curves accurately predict the experimental mechanical behavior of the hydrogels*

An *in silico* simple shear test was performed on the three fibered matrices reconstructed from the FIB-SEM images of the bovine collagen-based hydrogel. To fit the resulting curves to the experimental ones, the following bending and axial stiffness values were used during the tests: k_b=5.3·10^{-3} Pa·μm^4 and k_a=1.7·10^3 Pa·μm^2. These two parameters rely within the order of magnitude of single collagen fiber stiffness [64], reduce the number of phenomenological parameters of conventional hyperelastic laws used for hydrogels [65] and also remove the isotropy assumption.

It can be seen that the resulting curves are similar for the three VOIs (Fig. 3A), although not identical, as the corresponding fibered matrices

represented different regions of the global fibered matrix of the hydrogel (see the selection made in Fig. 2A). Nevertheless, the similarity of the results suggests that using other VOIs would yield equivalent outcomes. Furthermore, a non-linear mechanical behavior, typical of the simulated collagen hydrogels, is observed again in all three computational curves (as occurred in the experimental tests; see Fig. 3B). In particular, in the initial region of the curves, where deformations are low (approximately 0–10 % shear strain), bending stiffness dominates, representing the resistance of the fibers to deformation due to changes in their curvature. In this region, which exhibits approximately linear behavior, some fibers begin to uncoil or straighten and align with the direction of the applied load. Thus, the slope of the shear stress-strain curves in this region is governed primarily by the bending stiffness of the fibers. On the other hand, in regions with intermediate deformations, the fibers become more aligned with the load direction, reducing the influence of bending stiffness and increasing the effect of axial stiffness, which leads to non-linear behavior. This axial stiffness, which measures the resistance of the fibers to axial deformation under tensile or compression loads, improves the ability of the fibered matrix to withstand the applied load. Finally, at high levels of deformation (strain stiffening region, at the end of the tests), axial stiffness becomes the dominant factor. In that region, more fibers are fully or almost fully uncoiled and closely aligned with the load direction, resulting in an increase in shear stresses.

Fig. 3B shows the mean value of the three curves obtained from the VOIs, compared to the experimental results described in Section 3.1. It can be noted that this mean *in silico* test curve closely matched the experimental ones across the entire deformation range. This indicated that the reconstructed fibered matrices and their subsequent *in silico* tests were capable of accurately simulating both the real fibered matrix of the hydrogels and their non-linear mechanical behavior. Therefore, the FIB-SEM technique proved to be an effective tool for precisely reconstructing the fibrous nanostructure of the hydrogels. In this context, different studies have used imaging techniques to reconstruct fibrous networks with varying levels of detail. For example, Chen and Siegmund [44] used μCT images to model a 3D geometrically realistic fibrous network of a porous non-woven material for compression simulations. Similarly, Gaiselmann et al. [66] computationally generated the microstructure of compressed gas-diffusion layers, simulating the uniaxial compression of the fiber network. Other authors developed a methodology to characterize the topology of engineered fiber networks using SEM images and extracted parameters such as fiber orientation, connectivity or diameter [67]. In contrast, some studies focused on simplifications; for instance, reconstructing wood fiber networks from μCT and converting them into a Euclidean graph representation, which was then simplified for mechanical simulations [68]. In the present work, a step further is taken by employing FIB-SEM imaging, a state-of-the-art technique, to achieve a high-fidelity 3D reconstruction of a fibrous network at the nanometer scale while enabling the extraction of geometric parameters at the segment level into which the fibers are divided.

The state of the fibers of the three VOIs before (0 % shear strain), during (15 % shear strain) and after (30 % shear strain) performing the virtual simple shear tests is shown in Fig. 3C. Additionally, the complete *in silico* tests for VOIs 1, 2 and 3 are presented in Videos SM2, SM3 and SM4, respectively, in the supplementary material. The progressive deformation of the fibered matrices can be observed as the tests proceed, along with the formation of the shear stress-strain curves. Moreover, a different response was found between fibers oriented in the shear direction and those more perpendicular when applying the shear tests. While fibers oriented perpendicular to the shear direction tended to buckle, fibers aligned with the load experienced a stretching process (a similar analysis was discussed for a fibrin network in Ref. [69]).

In addition, in Fig. SM2 in the supplementary material, the histograms of the azimuthal (φ) and elevation (θ) angles of the segments (taking into account that the fibers were divided into segments during the reconstruction of the hydrogel network) are provided for the three VOIs prior to applying the virtual shear tests. These angles were obtained as described in Section 2.4. Regarding the orientation φ (Fig. SM2A), the angles spanned the entire range from 0° to 360° with relatively comparable frequencies, showing peak values at different angular positions depending on the VOI. In the case of the orientation θ (Fig. SM2B), the fiber segments adopted angles between 0° and 90°, indicating that they were distributed across all spatial angles. The most frequent orientation was near 90° (segment parallel to the X-Y plane), although significant and similar frequencies were found between approximately 30° and 85°. Orientations closer to 0° showed lower frequencies, revealing that few segments were aligned perpendicular to the X-Y plane. Overall, this suggests that the distributions were not uniform, though a broad range of angles with approximately constant probability was present.

3.3. Accumulated strain energy densities show dominant bending with increasing axial contribution

The accumulated strain energy densities developed by the fibered matrices are displayed in Fig. 4A. These energies were decomposed into axial, bending and torsional components. In the cited figure, the mean values of the energies across the considered VOIs are represented, along with the standard deviations. It can be observed that similar accumulated energies were obtained in the virtual tests of the three VOIs, as the standard deviations were small (the shaded areas are close to the mean curves), again indicating a consistent response among the VOIs. Bending energy dominated across the entire range of shear strain, playing a critical role in both uncoiling fibers and aligning them with the direction of the applied load. In contrast, axial energy became significant at approximately 15–20 % shear strain, corresponding to the straightening of certain fibers. However, torsional energy remained almost negligible throughout all three virtual tests.

Fig. 4B shows the mean energy fractions of the axial and bending components, as torsional contributions had little impact on the total accumulated energy. It can be seen that the bending and axial energies became comparable towards the end of the tests due to the effect of the axial stiffness and the straightened fibers. These results are qualitatively similar to others presented in the literature [70–72]. In those works, the evolution of bending and stretching energies was studied using computational fiber networks models. The results showed that, up to a certain point of deformation, the contribution of bending energy to the total elastic energy of the network was dominant. However, beyond this point of shear strain, stretching energy started to dominate. In the present study, a similar trend was observed, with the importance of bending energy decreasing and axial energy progressively increasing, although the transition point was not reached in the deformation range analyzed. In another 3D model of crosslinked F-actin filaments [73], it was also found that overall bending energy density governed at small strains, axial energy at large strains and that torsional energies were insignificant. In addition, Sanz-Herrera et al. [43] calculated the accumulated energies in a random fibered matrix subjected to a simple shear test, considering parameters defining the fibers and the axial and bending stiffnesses within the order of magnitude reported in the literature for biological fibrous networks. Their results also revealed a dominant bending energy and an increase in axial energy in the final stages of the test.

Finally, the evolution of the axial, bending and torsional accumulated energies in the fibers during the three virtual tests is shown in Videos SM5-13 (SM5-7 for VOI 1, SM8-10 for VOI 2 and SM11-13 for VOI 3) in the supplementary material. As an example, the axial and bending accumulated energies in the fibers of the VOI 1 are plotted in Fig. 4C at two points of deformation (during and after the shear test), since the torsional energies were approximately negligible. Again, it can be observed that the bending energy iss the highest and that the axial energy is mainly accumulated by the uncoiled fibers. At the end of the test, the maximum axial and bending energy values were of the same

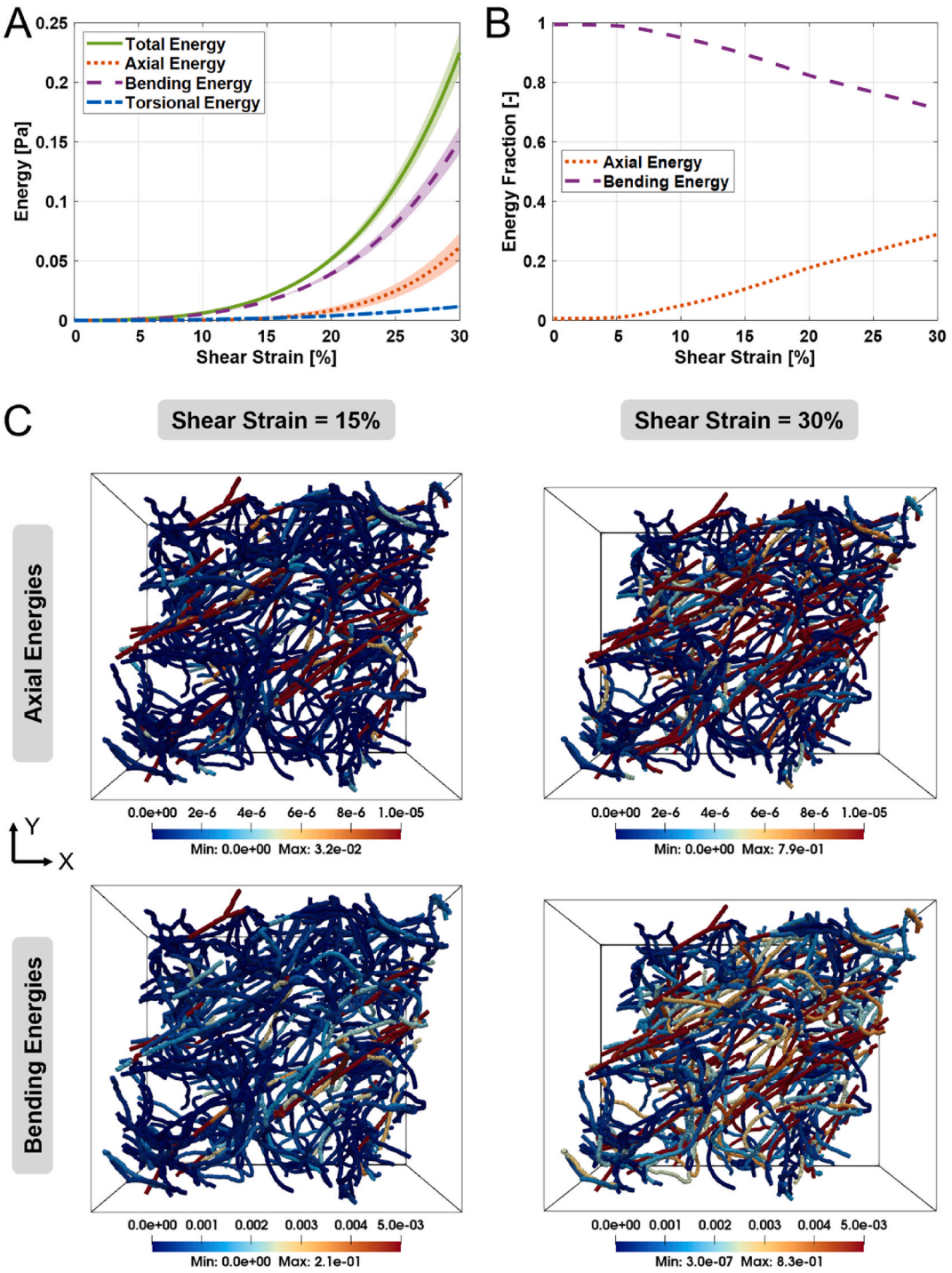

Fig. 4. Accumulated energies. A) Mean values (lines) and standard deviations (shaded areas) of the total, axial, bending and torsional accumulated strain energy densities developed by the fibered matrices of the volumes of interest in shear test. B) Fractions of the mean axial and bending energies with respect to the total energy (torsional energies were neglected). C) Axial and bending accumulated energies (in Pa·μm^3) at 15 % and 30 % shear strain in the fibers of the fibered matrix of the volume of interest 1.

order of magnitude and relatively similar. Equivalent analyses are performed with the other two VOIs (see the corresponding videos).

In summary, the proposed methodology enabled the calculation of the accumulated energies in the fibered matrices, revealing trends (Fig. 4A–B) similar to those reported in previous studies. Different from earlier models based on random fibrous networks, this approach considered real fiber structures and represented the distribution of each energy density component across all the fibers throughout the virtual experiments (Fig. 4C and corresponding videos). As far as the authors' knowledge, no other studies have computed these properties at this level of detail in a real network, making this a novel and accurate contribution to fiber network analysis.

3.4. Bending dominates total stresses, while straightened fibers develop the majority of axial stresses

In this section, the total, axial and bending stresses calculated during the virtual tests are presented. The evolution of these stresses in each

element of the fibers of the three VOIs is displayed in Videos SM14-22 (SM14-16 for VOI 1, SM17-19 for VOI 2 and SM20-22 for VOI 3) in the supplementary material. Moreover, in an equivalent manner to Section 3.3, the stresses developed in the fibers of the VOI 1 at two points of deformation are plotted in Fig. 5 (at 15 % and 30 % shear strain). By analyzing the axial stresses, it can be seen that the straightened fibers developed the majority of this stress (with positive values and reddish colors), while the buckled fibers exhibited negative stress values (represented by bluish colors in the figure). At the end of the test, the minimum axial stresses (in absolute values) were approximately an order of magnitude lower than the maximum ones. Similar to the energy results, the bending stresses were the most significant during the simple shear test and also showed high values in the uncoiled fibers, with maximum values approximately three times higher than the maximum axial stress at 30 % shear strain. Finally, the total stresses resulted from the sum of the two previous stresses, with the bending stress added when the axial stress was positive and subtracted when the axial stress was negative. Once again, a clear difference in magnitude was observed between the maximum and minimum total stresses (in absolute values) when the test was completed. This analysis would be equivalent for the VOIs 2 and 3

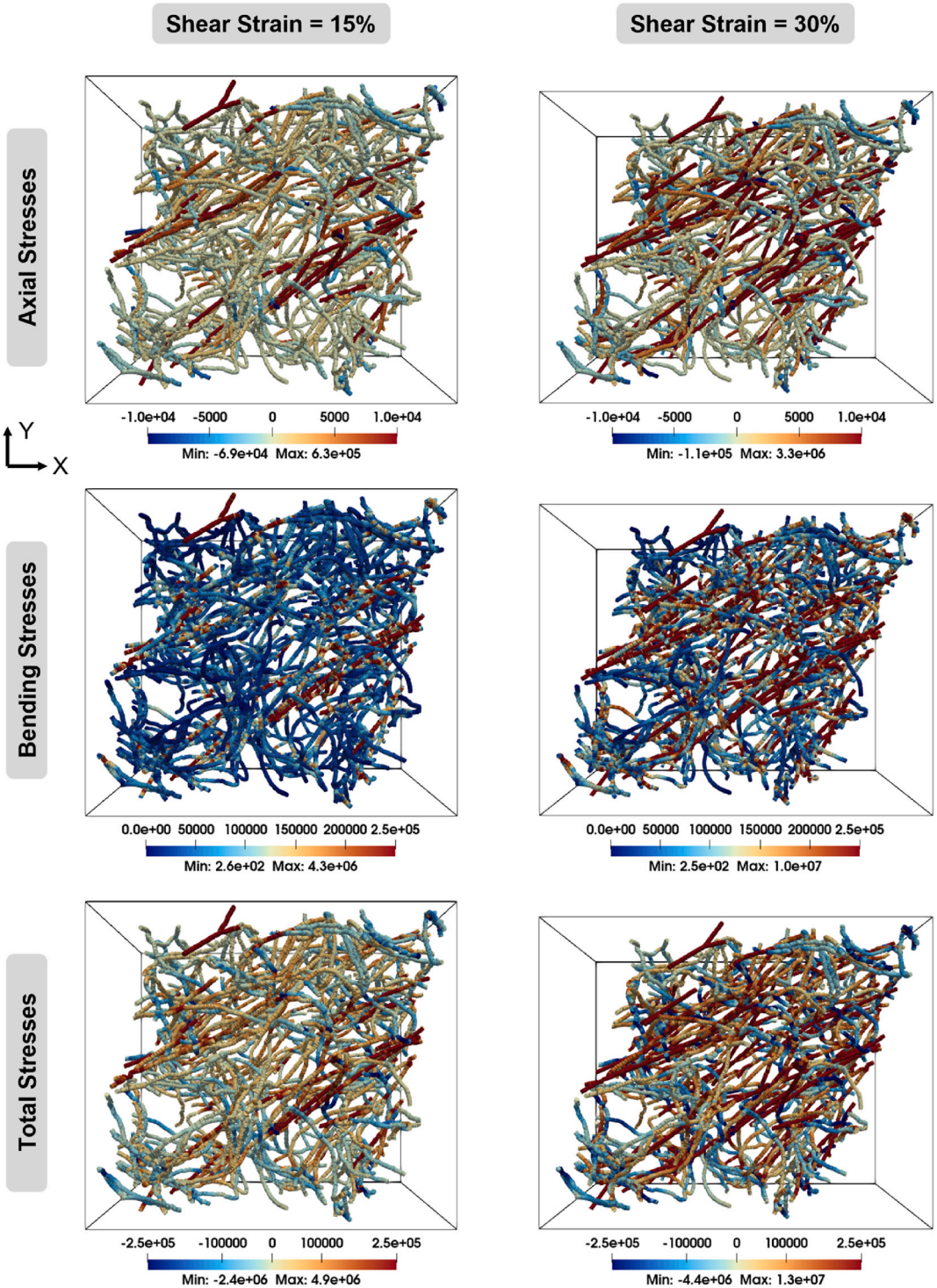

Fig. 5. Axial, bending and total stresses (in Pa) at 15 % and 30 % shear strain in the fibers of the fibered matrix of the volume of interest 1 in shear test.

(see the corresponding videos).

4. Conclusions

In this work, a methodology was developed to precisely reproduce *in silico* the mechanical behavior of collagen-based hydrogels as observed in experimental studies. For this purpose, the real nanostructure of bovine dermis collagen hydrogels was accurately reconstructed using FIB-SEM images of the hydrogels, assuming that the dehydration process had limited influence on the fiber nanoarchitecture. This represents a novel method for reconstructing the nanostructure of a fibrous material, offering a more accurate network than other previous image-based models that simplify the structure. Three different inner volumes of interest were selected from the reconstructed network, and a multiscale model was employed to perform *in silico* shear tests on these volumes. Therefore, this methodology provided a framework to elucidate the structure-mechanical behavior relationship of the fiber network topology.

The results of the experimental tests were qualitatively consistent with findings reported in the literature, while the virtual tests conducted on the three volumes of interest produced results comparable to the experimental ones. In particular, this methodology successfully replicated the experimental shear stress-strain curves of the collagen hydrogels, capturing their characteristic non-linear behavior from the fibrous network nanostructures. Additionally, the model predicted that bending energy was the most significant within the analyzed deformation range. This was attributed to the stretching and alignment of certain collagen fibers along the load direction during the tests. In contrast, axial energy became increasingly significant after the transition to non-linear mechanical behavior, corresponding to the straightening of specific fibers. Moreover, to the best of the authors' knowledge, this was the first study to analyze and represent the evolution of axial and bending stresses in each element of a real fiber network, which could provide useful information that complements the understanding of the mechanical behavior of this type of network.

In summary, this work has the advantage and novelty of enabling the *in silico* reconstruction of the real fibered matrix of a hydrogel at the nanometer scale, taking into account the varying lengths and tortuosities of the fibers, as well as the simulation of its mechanical behavior. Although the proposed methodology was applied to specific collagen-based hydrogels, it can be extended to other types of hydrogels and fiber networks in different engineering materials. For instance, it could be employed for soft tissues, which typically exhibit higher stresses and accumulated energies. In addition, this approach also allows for studying the apparent mechanical properties of degraded and/or remodeled hydrogels based on FIB-SEM images. Therefore, future work will focus on extending this methodology to other materials and tissue types, also expanding the range of mechanical tests to reproduce the response under tensile and compressive loading conditions.

CRediT authorship contribution statement

Elías Núñez-Ortega: Writing – review & editing, Writing – original draft, Visualization, Validation, Methodology, Investigation, Formal analysis, Data curation. **Pablo Blázquez-Carmona:** Writing – review & editing, Writing – original draft, Visualization, Validation, Supervision, Methodology, Investigation, Formal analysis, Data curation. **Raquel Ruiz-Mateos:** Validation, Methodology, Investigation, Data curation. **José E. Martín-Alfonso:** Writing – review & editing, Resources. **José A. Sanz-Herrera:** Writing – review & editing, Writing – original draft, Visualization, Validation, Supervision, Software, Project administration, Methodology, Investigation, Formal analysis, Conceptualization. **Esther Reina-Romo:** Writing – review & editing, Writing – original draft, Visualization, Validation, Supervision, Software, Project administration, Methodology, Investigation, Funding acquisition, Formal analysis, Conceptualization.

Declaration of competing interest

The authors declare that they have no known competing financial interests or personal relationships that could have appeared to influence the work reported in this paper.

Acknowledgments

This study was supported by the MICIU (Ministry of Science, Innovation and Universities of the Spanish Government) and ERPF/EU (European Regional Development Fund of the European Union) via Grant PID 2023-148828OB-I00 funded by MICIU/AEI/10.13039/501100011033 and by the ERDF/EU. Elías Núñez-Ortega was supported by grant PREP2023-001306.

Appendix A. Supplementary data

Supplementary data to this article can be found online at https://doi.org/10.1016/j.mtbio.2025.101962.

Data availability

Data will be made available on request.

References

[1] G.A. Holzapfel, Biomechanics of soft tissue, in: J. Lemaitre (Ed.), Handbook of Materials Behavior Models, Academic Press, 2001, pp. 1049–1063, https://doi.org/10.1016/B978-012443341-0/50107-1.
[2] C. Zhao, Y. Xiao, S. Ling, Y. Pei, J. Ren, Structure of collagen, in: S. Ling (Ed.), Fibrous Proteins: Design, Synthesis, and Assembly, Springer US, New York, NY, 2021, pp. 17–25, https://doi.org/10.1007/978-1-0716-1574-4_2.
[3] J. Xiao, The collagen suprafamily, in: Collagen Mimetic Peptides and Their Biophysical Characterization, Springer, Singapore, 2024, pp. 1–24, https://doi.org/10.1007/978-981-10-1941-8_1.
[4] A. Owczarzy, R. Kurasiński, K. Kulig, W. Rogóż, A. Szkudlarek, M. Maciążek-Jurczyk, Collagen - structure, properties and application, Eng. Biomater. 23 (2020) 17–23, https://doi.org/10.34821/eng.biomat.156.2020.17-23.
[5] M. Shenoy, N.S. Abdul, Z. Qamar, B.M. Al Bahri, K.Z.K. Al Ghalayini, A. Kakti, Collagen structure, synthesis, and its applications: a systematic review, Cureus 14 (2022) e24856, https://doi.org/10.7759/cureus.24856.
[6] Y. Nakashima, Pathogenesis of aortic dissection: elastic fiber abnormalities and aortic medial weakness, Ann. Vasc. Dis. 3 (2010) 28–36, https://doi.org/10.3400/avd.ctiia09001.
[7] L.F. Borges, J.P.F. Blini, R.R. Dias, P.S. Gutierrez, Why do aortas cleave or dilate? Clues from an electronic scanning microscopy study in human ascending aortas, J. Vasc. Res. 51 (2014) 50–57, https://doi.org/10.1159/000356296.
[8] J. Tong, T. Cohnert, G.A. Holzapfel, Diameter-related variations of geometrical, mechanical, and mass fraction data in the anterior portion of abdominal aortic aneurysms, Eur. J. Vasc. Endovasc. Surg. 49 (2015) 262–270, https://doi.org/10.1016/j.ejvs.2014.12.009.
[9] S. Saarakkala, P. Julkunen, P. Kiviranta, J. Mäkitalo, J.S. Jurvelin, R.K. Korhonen, Depth-wise progression of osteoarthritis in human articular cartilage: investigation of composition, structure and biomechanics, Osteoarthr. Cartil. 18 (2010) 73–81, https://doi.org/10.1016/j.joca.2009.08.003.
[10] J.A. Buckwalter, H.J. Mankin, Articular cartilage. Part II: degeneration and osteoarthritis, repair, regeneration and transplantation, J. Bone Joint Surg. 79 (1997) 612–632.
[11] N.D. Broom, T. Ngo, E. Tham, Traversing the intact/fibrillated joint surface: a biomechanical interpretation, J. Anat. 206 (2005) 55–67, https://doi.org/10.1111/j.0021-8782.2005.00371.x.
[12] X. Bi, G. Li, S.B. Doty, N.P. Camacho, A novel method for determination of collagen orientation in cartilage by Fourier transform infrared imaging spectroscopy (FT-IRIS), Osteoarthr. Cartil. 13 (2005) 1050–1058, https://doi.org/10.1016/j.joca.2005.07.008.
[13] N.D. Broom, The altered biomechanical state of human femoral head osteoarthritic articular cartilage, Arthritis Rheum. 27 (1984) 1028–1039, https://doi.org/10.1002/art.1780270910.
[14] X. Bi, X. Yang, M.P.G. Bostrom, N.P. Camacho, Fourier transform infrared imaging spectroscopy investigations in the pathogenesis and repair of cartilage, Biochim. Biophys. Acta 1758 (2006) 934–941, https://doi.org/10.1016/j.bbamem.2006.05.014.
[15] C. Bonnans, J. Chou, Z. Werb, Remodelling the extracellular matrix in development and disease, Nat. Rev. Mol. Cell Biol. 15 (2014) 786–801, https://doi.org/10.1038/nrm3904.
[16] I. Acerbi, L. Cassereau, I. Dean, Q. Shi, A. Au, C. Park, Y.Y. Chen, J. Liphardt, E. S. Hwang, V.M. Weaver, Human breast cancer invasion and aggression correlates

with ECM stiffening and immune cell infiltration, Integr. Biol. 7 (2015) 1120–1134, https://doi.org/10.1039/c5ib00040h.
[17] J.C. Ashworth, J.L. Thompson, J.R. James, C.E. Slater, S. Pijuan-Galitó, K. Lis-Slimak, R.J. Holley, K.A. Meade, A. Thompson, K.P. Arkill, M. Tassieri, A.J. Wright, G. Farnie, C.L.R. Merry, Peptide gels of fully-defined composition and mechanics for probing cell-cell and cell-matrix interactions in vitro, Matrix Biol. 85–86 (2020) 15–33, https://doi.org/10.1016/j.matbio.2019.06.009.
[18] N. Gjorevski, N. Sachs, A. Manfrin, S. Giger, M.E. Bragina, P. Ordóñez-Morán, H. Clevers, M.P. Lutolf, Designer matrices for intestinal stem cell and organoid culture, Nature 539 (2016) 560–564, https://doi.org/10.1038/nature20168.
[19] A. Micalet, E. Moeendarbary, U. Cheema, 3D in vitro models for investigating the role of stiffness in cancer invasion, ACS Biomater. Sci. Eng. 9 (2023) 3729–3741, https://doi.org/10.1021/acsbiomaterials.0c01530.
[20] J.C. Ashworth, T.R. Cox, The importance of 3D fibre architecture in cancer and implications for biomaterial model design, Nat. Rev. Cancer 24 (2024) 461–479, https://doi.org/10.1038/s41568-024-00704-8.
[21] E. Rezvani Ghomi, N. Nourbakhsh, M. Akbari Kenari, M. Zare, S. Ramakrishna, Collagen-based biomaterials for biomedical applications, J. Biomed. Mater. Res. B Appl. Biomater. 109 (2021) 1986–1999, https://doi.org/10.1002/jbm.b.34881.
[22] M.C. Catoira, L. Fusaro, D. Di Francesco, M. Ramella, F. Boccafoschi, Overview of natural hydrogels for regenerative medicine applications, J. Mater. Sci. Mater. Med. 30 (2019) 115, https://doi.org/10.1007/s10856-019-6318-7.
[23] H. Wosicka-Frąckowiak, K. Poniedziałek, S. Woźny, M. Kuprianowicz, M. Nyga, B. Jadach, B. Milanowski, Collagen and its derivatives serving biomedical purposes: a review, Polymers (Basel) 16 (2024) 2668, https://doi.org/10.3390/polym16182668.
[24] J. She, J. Liu, Y. Mu, S. Lv, J. Tong, L. Liu, T. He, J. Wang, D. Wei, Recent advances in collagen-based hydrogels: materials, preparation and applications, React. Funct. Polym. 207 (2025) 106136, https://doi.org/10.1016/j.reactfunctpolym.2024.106136.
[25] E.E. Antoine, P.P. Vlachos, M.N. Rylander, Review of collagen I hydrogels for bioengineered tissue microenvironments: characterization of mechanics, structure, and transport, Tissue Eng., Part B 20 (2014) 683–696, https://doi.org/10.1089/ten.teb.2014.0086.
[26] S.O. Sarrigiannidis, J.M. Rey, O. Dobre, C. González-García, M.J. Dalby, M. Salmeron-Sanchez, A tough act to follow: collagen hydrogel modifications to improve mechanical and growth factor loading capabilities, Mater. Today Bio 10 (2021) 100098, https://doi.org/10.1016/j.mtbio.2021.100098.
[27] D.K. Baby, Rheology of hydrogels, in: S. Thomas, C. Sarathchandran, N. Chandran (Eds.), Rheology of Polymer Blends and Nanocomposites, Elsevier, Amsterdam, The Netherlands, 2020, pp. 193–204, https://doi.org/10.1016/B978-0-12-816957-5.00009-4.
[28] G. Stojkov, Z. Niyazov, F. Picchioni, R.K. Bose, Relationship between structure and rheology of hydrogels for various applications, Gels 7 (2021) 255, https://doi.org/10.3390/gels7040255.
[29] E. Sozumert, V.V. Silberschmidt, Numerical models of random fibrous networks, in: V.V. Silberschmidt (Ed.), Mechanics of Fibrous Networks, Elsevier, 2022, pp. 113–143, https://doi.org/10.1016/B978-0-12-822207-2.00012-X.
[30] X. He, M.R. Islam, F. Ji, B. Wang, I.A. Sigal, Comparing continuum and direct fiber models of soft tissues: an ocular biomechanics example reveals that continuum models may artificially disrupt the strains at both the tissue and fiber levels, Acta Biomater. 190 (2024) 317–328, https://doi.org/10.1016/j.actbio.2024.10.019.
[31] M. Aghvami, K.L. Billiar, E.A. Sander, Fiber network models predict enhanced cell mechanosensing on fibrous gels, J. Biomech. Eng. 138 (2016) 1010061–10100611, https://doi.org/10.1115/1.4034490.
[32] M.B. Rubin, S.R. Bodner, A three-dimensional nonlinear model for dissipative response of soft tissue, Int. J. Solid Struct. 39 (2002) 5081–5099, https://doi.org/10.1016/S0020-7683(02)00237-8.
[33] T. Jin, I. Stanciulescu, Numerical simulation of fibrous biomaterials with randomly distributed fiber network structure, Biomech. Model. Mechanobiol. 15 (2016) 817–830, https://doi.org/10.1007/s10237-015-0725-6.
[34] B.A. Lane, K.A. Harmon, R.L. Goodwin, M.J. Yost, T. Shazly, J.F. Eberth, Constitutive modeling of compressible type-I collagen hydrogels, Med. Eng. Phys. 53 (2018) 39–48, https://doi.org/10.1016/j.medengphy.2018.01.003.
[35] A.P.G. Castro, P. Laity, M. Shariatzadeh, C. Wittkowske, C. Holland, D. Lacroix, Combined numerical and experimental biomechanical characterization of soft collagen hydrogel substrate, J. Mater. Sci. Mater. Med. 27 (2016) 79, https://doi.org/10.1007/s10856-016-5688-3.
[36] A.P.G. Castro, J. Yao, T. Battisti, D. Lacroix, Poroelastic modeling of highly hydrated collagen hydrogels: experimental results vs. Numerical simulation with custom and commercial finite element solvers, Front. Bioeng. Biotechnol. 6 (2018) 142, https://doi.org/10.3389/fbioe.2018.00142.
[37] X. Hou, M. Acar, V.V. Silberschmidt, 2D finite element analysis of thermally bonded nonwoven materials: continuous and discontinuous models, Comput. Mater. Sci. 46 (2009) 700–707, https://doi.org/10.1016/j.commatsci.2009.07.007.
[38] H. Altendorf, D. Jeulin, Random-walk-based stochastic modeling of three-dimensional fiber systems, Phys. Rev. E 83 (2011) 041804, https://doi.org/10.1103/PhysRevE.83.041804.
[39] R.Y. Kwon, A.J. Lew, C.R. Jacobs, A microstructurally informed model for the mechanical response of three-dimensional actin networks, Comput. Methods Biomech. Biomed. Eng. 11 (2008) 407–418, https://doi.org/10.1080/10255840801888686.
[40] K. Berkache, S. Deogekar, I. Goda, R.C. Picu, J.F. Ganghoffer, Construction of second gradient continuum models for random fibrous networks and analysis of size effects, Compos. Struct. 181 (2017) 347–357, https://doi.org/10.1016/j.compstruct.2017.08.078.
[41] B. Lee, X. Zhou, K. Riching, K.W. Eliceiri, P.J. Keely, S.A. Guelcher, A.M. Weaver, Y. Jiang, A three-dimensional computational model of collagen network mechanics, PLoS One 9 (2014) e111896, https://doi.org/10.1371/journal.pone.0111896.
[42] S. Dong, Z. Huang, L. Tang, X. Zhang, Y. Zhang, Y. Jiang, A three-dimensional collagen-fiber network model of the extracellular matrix for the simulation of the mechanical behaviors and micro structures, Comput. Methods Biomech. Biomed. Eng. 20 (2017) 991–1003, https://doi.org/10.1080/10255842.2017.1321113.
[43] J.A. Sanz-Herrera, A. Apolinar-Fernandez, A. Jimenez-Aires, P. Perez-Alcantara, J. Dominguez, E. Reina-Romo, Multiscale characterization of the mechanics of curved fibered structures with application to biological and engineered materials, Comput. Struct. 310 (2025) 107690, https://doi.org/10.1016/j.compstruc.2025.107690.
[44] Y. Chen, T. Siegmund, Mechanics of compaction of a porous non-woven fiber solid, Mech. Mater. 137 (2019) 103101, https://doi.org/10.1016/j.mechmat.2019.103101.
[45] M. Faessel, C. Delisée, F. Bos, P. Castéra, 3D Modelling of random cellulosic fibrous networks based on X-ray tomography and image analysis, Compos. Sci. Technol. 65 (2005) 1931–1940, https://doi.org/10.1016/j.compscitech.2004.12.038.
[46] S.B. Lindström, D.A. Vader, A. Kulachenko, D.A. Weitz, Biopolymer network geometries: characterization, regeneration, and elastic properties, Phys. Rev. E 82 (2010) 051905, https://doi.org/10.1103/PhysRevE.82.051905.
[47] V. Olivares, M. Cóndor, C. Del Amo, J. Asín, C. Borau, J.M. García-Aznar, Image-based characterization of 3D collagen networks and the effect of embedded cells, Microsc. Microanal. 25 (2019) 971–981, https://doi.org/10.1017/S1431927619014570.
[48] A. D'Amore, N. Amoroso, R. Gottardi, C. Hobson, C. Carruthers, S. Watkins, W. R. Wagner, M.S. Sacks, From single fiber to macro-level mechanics: a structural finite-element model for elastomeric fibrous biomaterials, J. Mech. Behav. Biomed. Mater. 39 (2014) 146–161, https://doi.org/10.1016/j.jmbbm.2014.07.016.
[49] S. Deogekar, M.R. Islam, R.C. Picu, Parameters controlling the strength of stochastic fibrous materials, Int. J. Solid Struct. 168 (2019) 194–202, https://doi.org/10.1016/j.ijsolstr.2019.03.033.
[50] E. Ban, V.H. Barocas, M.S. Shephard, C.R. Picu, Effect of fiber crimp on the elasticity of random fiber networks with and without embedding matrices, J. Appl. Mech. 83 (2016) 041008, https://doi.org/10.1115/1.4032465.
[51] J. Hao, R.A. Weiss, Viscoelastic and mechanical behavior of hydrophobically modified hydrogels, Macromolecules 44 (2011) 9390–9398, https://doi.org/10.1021/ma202130u.
[52] C. Yan, D.J. Pochan, Rheological properties of peptide-based hydrogels for biomedical and other applications, Chem. Soc. Rev. 39 (2010) 3528–3540, https://doi.org/10.1039/b919449p.
[53] J. Yang, C.R. Han, J.F. Duan, F. Xu, R.C. Sun, Mechanical and viscoelastic properties of cellulose nanocrystals reinforced poly(ethylene glycol) nanocomposite hydrogels, ACS Appl. Mater. Interfaces 5 (2013) 3199–3207, https://doi.org/10.1021/am4001997.
[54] A.G. Marshall, S.M. Damo, A. Hinton, Revisiting focused ion beam scanning electron microcopy, Trends Biochem. Sci. 48 (2023) 585–586, https://doi.org/10.1016/j.tibs.2023.02.005.
[55] C. Kizilyaprak, J. Daraspe, B.M. Humbel, Focused ion beam scanning electron microscopy in biology, J. Microsc. 254 (2014) 109–114, https://doi.org/10.1111/jmi.12127.
[56] P. Blázquez-Carmona, R. Ruiz-Mateos, J. Barrasa-Fano, A. Shapeti, J.E. Martín-Alfonso, J. Domínguez, H. Van Oosterwyck, E. Reina-Romo, J.A. Sanz-Herrera, Quantitative atlas of collagen hydrogels reveals mesenchymal cancer cell traction adaptation to the matrix nanoarchitecture, Acta Biomater. 185 (2024) 281–295, https://doi.org/10.1016/j.actbio.2024.07.002.
[57] J.M. Serra Lleti, Automated Correlative Light and Electron Microscopy Using FIB-SEM as a Tool to Screen for Ultrastructural Phenotypes, Ruperto-Carola University of Heidelberg, 2020, https://doi.org/10.11588/heidok.00026154. Doctoral dissertation.
[58] R. Alberini, A. Spagnoli, M.J. Sadeghinia, B. Skallerud, M. Terzano, G.A. Holzapfel, Fourier transform-based method for quantifying the three-dimensional orientation distribution of fibrous units, Sci. Rep. 14 (2024) 1999, https://doi.org/10.1038/s41598-024-51550-5.
[59] J.A.J. Van Der Rijt, K.O. Van Der Werf, M.L. Bennink, P.J. Dijkstra, J. Feijen, Micromechanical testing of individual collagen fibrils, Macromol. Biosci. 6 (2006) 697–702, https://doi.org/10.1002/mabi.200600063.
[60] C.A. Grant, D.J. Brockwell, S.E. Radford, N.H. Thomson, Tuning the elastic modulus of hydrated collagen fibrils, Biophys. J. 97 (2009) 2985–2992, https://doi.org/10.1016/j.bpj.2009.09.010.
[61] M. Marino, P. Wriggers, Finite strain response of crimped fibers under uniaxial traction: an analytical approach applied to collagen, J. Mech. Phys. Solid. 98 (2017) 429–453, https://doi.org/10.1016/j.jmps.2016.05.010.
[62] R.C. Arevalo, P. Kumar, J.S. Urbach, D.L. Blair, Stress heterogeneities in sheared type-I collagen networks revealed by boundary stress microscopy, PLoS One 10 (2015) e0118021, https://doi.org/10.1371/journal.pone.0118021.
[63] P.A. Janmey, M.E. McCormick, S. Rammensee, J.L. Leight, P.C. Georges, F. C. MacKintosh, Negative normal stress in semiflexible biopolymer gels, Nat. Mater. 6 (2007) 48–51, https://doi.org/10.1038/nmat1810.
[64] J.S. Graham, A.N. Vomund, C.L. Phillips, M. Grandbois, Structural changes in human type I collagen fibrils investigated by force spectroscopy, Exp. Cell Res. 299 (2004) 335–342, https://doi.org/10.1016/j.yexcr.2004.05.022.

[65] J. Steinwachs, C. Metzner, K. Skodzek, N. Lang, I. Thievessen, C. Mark, S. Münster, K.E. Aifantis, B. Fabry, Three-dimensional force microscopy of cells in biopolymer networks, Nat. Methods 13 (2016) 171–176, https://doi.org/10.1038/nmeth.3685.
[66] G. Gaiselmann, C. Tötzke, I. Manke, W. Lehnert, V. Schmidt, 3D microstructure modeling of compressed fiber-based materials, J. Power Sources 257 (2014) 52–64, https://doi.org/10.1016/j.jpowsour.2014.01.095.
[67] A. D'Amore, J.A. Stella, W.R. Wagner, M.S. Sacks, Characterization of the complete fiber network topology of planar fibrous tissues and scaffolds, Biomaterials 31 (2010) 5345–5354, https://doi.org/10.1016/j.biomaterials.2010.03.052.
[68] M. Alimadadi, S.B. Lindström, A. Kulachenko, Role of microstructures in the compression response of three-dimensional foam-formed wood fiber networks, Soft Matter 14 (2018) 8945–8955, https://doi.org/10.1039/C7SM02561K.
[69] S. Münster, L.M. Jawerth, B.A. Leslie, J.I. Weitz, B. Fabry, D.A. Weitz, Strain history dependence of the nonlinear stress response of fibrin and collagen networks, Proc. Natl. Acad. Sci. USA. 110 (2013) 12197–12202, https://doi.org/10.1073/pnas.1222787110.
[70] H. Hatami-Marbini, M. Rohanifar, Nonlinear mechanical properties of prestressed branched fibrous networks, Biophys. J. 120 (2021) 527–538, https://doi.org/10.1016/j.bpj.2020.10.050.
[71] M. Vahabi, A. Sharma, A.J. Licup, A.S.G. van Oosten, P.A. Galie, P.A. Janmey, F. C. MacKintosh, Elasticity of fibrous networks under uniaxial prestress, Soft Matter 12 (2016) 5050–5060, https://doi.org/10.1039/c6sm00606j.
[72] B. Sun, The mechanics of fibrillar collagen extracellular matrix, Cell Rep. Phys. Sci. 2 (2021) 100515, https://doi.org/10.1016/j.xcrp.2021.100515.
[73] E.M. Huisman, T. van Dillen, P.R. Onck, E. Van der Giessen, Three-dimensional cross-linked F-actin networks: relation between network architecture and mechanical behavior, Phys. Rev. Lett. 99 (2007) 208103, https://doi.org/10.1103/PhysRevLett.99.208103.